Monitoring Land Surface Temperature (LST) and Land Cover of Basra Province using Remote Sensing Technique and GIS

Kawther Salman[1a*] and Ban A. Al Razaq[1b]

[1]Department of Remote Sensing, College of Science, University of Baghdad, Baghdad, Iraq
[b]E-mail: Dr.ban1969@gmail.com
[a*]Corresponding author: kawtharsalman9797@gmail.com

Abstract

   This study investigates the changes occurring in the province of Basra using geospatial methods and analyzes the variations in land surface temperature among the various types of land cover. For the months of July and December in the years 2013 and 2021, Landsat images were used in Landsat 8 OLI/TIRS, and satellite images were processed using ArcGIS 10.8 software. The study's categories for land use and land cover were generated through the application of supervised classification techniques, and the land surface temperature was calculated using data from a satellite sensor's brightness temperature. According to the study's findings, there has been an increase in urban area, (including barren land). From 2013 to 2021, a greater correlation between urban land and LST was found, indicating an increasing surface urban heat island effect as evidenced by its statistically significant correlation coefficients. It has a significant impact on the variations in land surface temperature. This study also highlighted the key variations in how land use and cover affect LST. Across all time periods of investigation. Therefore, techniques for remote sensing and geographic information systems are useful for tracking and analyzing urban expansion patterns and assessing their effects on land surface temperature.

1. Introduction

   The abrupt climate change in urban areas has recently become increasingly substantial and evident due to changes in Land Use Land Cover (LULC) and anthropogenic activities carried out by humans [1, 2]. For instance, Land Surface Temperature (LST) is higher in urban areas than in rural areas. These changes happened after vegetative surfaces were changed and modified to impervious surfaces, such as asphalt, concrete, tars, etc. The thermal conductivity and radiation heat budget in metropolitan areas is typically higher. As a result, if rural-to-urban conversion is drastic, LST may be higher in urban areas. Recently, this acceleration has caused LULC concerns generating declines in the productivity and responsiveness of terrestrial ecosystems and losses in biological diversity, water quality, and air quality [3, 4]. LST and the air temperature stated in the daily weather report are not the same. The activity of the planet's thermal system is largely influenced by LST, which controls the effective radiative temperature of the Earth's surface. Due to the extreme heterogeneity of most natural land surfaces, it is difficult to quantify and validate this parameter. Land surface temperature (LST) indicators are increasingly used as useful study tools in discussions of regional energy change. LST is an effective indicator for analyzing environmental circumstances [5, 6]. Studies on LST changes in road regions are presently less common than studies on LST changes in various urban areas. Because it is an important indicator of environmental change, most LST researchers use it as a key characterization parameter for surface energy evolution and environmental change. However, researchers have made it simpler to use satellite data in conjunction with real-time

monitoring and measurement methods to examine regional LST [7, 8]. Most of the reported studies, presently, only address the LST of urban regional road networks and strongly emphasize urban areas. However, due to its own changes, in-depth research and analysis should be carried out to focus on sustainable growth as a crucial aspect of creating a social foundation. Internal analysis of the LST of the regional road network area and analysis of the evolution of the influence mechanism of the LST along the road during its constantly changing process was performed using Landsat 8 remote sensing image data [9]. LST has historically been directly measurable from the ground truth. Nevertheless, this approach is quite time-consuming and only covers a limited area. The recovery of LST directly from a satellite image has grown in popularity in recent years due to the availability of numerous and varied satellite images. The covering area is wider and takes less time than the ground truth measurement. But once LST has been collected, ground truth measurement data must be used to verify its value.

This study aims to determine the changes in the Land Surface Temperature (LST) of Basra governorate in the years 2013 and 2021.

2. Classification Techniques

Each pixel in an image or the original remotely sensed satellite data is classified according to its kind in a process known as "classification", which aims to produce a good collection of land cover information. Based on the various land features, the classification is influenced by the studied region's (rural or urban) nature, which makes each spectral category unique. Classification differs from other species through its unique reflectance and diffusion characteristics. Modern classification techniques, including supervised and unsupervised methods, are commonly used to produce land cover maps [10, 11].

2.1. Supervised Classification

A form of machine learning known as supervised classification uses predetermined training samples and a classification algorithm. The classification algorithm most often used in supervised remote sensing is the classification process. The supervised part is the most compelling portion of the Landsat image categorization technique and is the sample for training. The accuracy categorization is strongly reliant on the training samples chosen; when you are done with this; you will have a finished product. The categorization accuracy is strongly dependent on the training examples selected. A classification is given to every class, which the business refers to as training. In supervised categorization, the user must pick a region of interest. This will serve as a classifier in the image. All pixels in the image will be utilized [12]. The quality of the supervised categorization is based on the caliber of the training locations. In the majority of supervised categories, there is a set of steps that must be followed:

a- Define the training sites.

b- Extract signatures.

c- Maximum Likelihood Classification (MLC).

d- Calculate Area.

The training spaces were created using digital elements. This method ensures that the data is accurate, the classification is valid, and the interpretation of the data is accurate. Typically, four training sites were used; the more training sites chosen, the better the results. Statistical information was gathered following the digitalization of the training site regions. Data characterizations were created, and one technique of

supervised classification called Maximum Likelihood Classification (MLC) was applied [13, 14]. This technique uses a simple pattern, expected on the likelihood that a pixel will fit into a specific category or class, and training locations are selected by the user. The most common classification in remote sensing is based on the basic premise that all groups have equal probabilities. An image's spectral classes are represented by:

$$\omega_i, i = 1, \ldots\ldots\ldots\ldots M$$

where M represents the overall amount of classes. It is strictly the conditional probabilities that decide the class or category to which a pixel vector x belongs.

$$p(\omega_i|x), i = 1, \ldots\ldots\ldots\ldots M$$

The column of luminance values for the pixel makes up the measurement vector x. A spot in multispectral space with coordinates determined by brightness is how the pixel is described. The likelihood that the right class is i for a pixel at position x is given by the probability $p(\omega_i|x)$. Classification is carried out in accordance with the relation [15]:

$$x \in \omega_i, \text{if } p(\omega_i|x) > p(\omega_j|x) \text{for all } j = i \tag{1}$$

3. The Thermal Band Method Used by Landsat 8 to Determine Surface Temperature

As shown in Fig. 1, the proportional vegetation PV, emissivity E, and blackbody brightness of the features were calculated using the NDVI-based technique to determine Land Surface Temperature (LST). The working steps are:

1- The sensor spectral radiance (LS) was determined by changing the digital number (DN) values to absolute radiance under the assumption that the thermal band pixels in Landsat images (B10 for Landsat 8) is converted to sensor spectral radiance (LS) using the formula [16]:

$$LS = \text{gain} \times DN + \text{bias} \tag{2}$$

where, for Landsat-8: gain=0.0003342, bias = 0.1[10].

2- Radiation (TIRS) is converted to at-satellite Brightens Temperature (BT). Planck's Law, inverted and calibration values for Landsat-8/bands 10 (K1=774.89, K2=1321.08), and 11 (K1=480.8883, K2=1201.1442), to calculate brightness temperature (BT) [12] according to the equation [3]:

$$BT = K2/\ln(K1/LS + 1) \tag{3}$$

where K1 and K2 are the TIR's thermal constants, which can be located in the metadata file attached to the satellite images.

3- In order to determine whether there is live, lush vegetation present, the Normalized Difference Vegetation Index (NDVI) was determined by a simple numerical measure, from -1 to +1, which is known as the NDVI scale. The NDVI was calculated per-pixel as the normalized difference between the red band of a picture (0.64-0.67µm) and the near-infrared band (0.85-0.88µm). Applying bands 4 (Red band) and 5 (NIR band) from Landsat 8 images, the following equation is used to compute NDVI [17, 18]:

$$NDVI = \left(\frac{NIR - Red}{NIR + Red}\right) \tag{4}$$

when the Normalized Difference Vegetation Index (NDVI) is used, red denotes the red band, while NIR stands for near-infrared (band).

4- Using the NDVI readings, the proportional vegetation (PV) was determined. To calculate LST, one needs to know the land surface emissivity (E), which defines a surface's capacity to absorb radiation in the logarithmic waveband. The target surface top layer, including the type of soil, surface roughness, and the type of plant cover, strongly influences the land surface emissivity. This proportional vegetation estimates the area covered by each variety of land cover. The NDVI of pure pixels is used to calculate the amounts of vegetation and bare earth. Eq. (5) can be used to determine PV [19, 20]:

$$PV = ((NDVI - NDVImin)/(NDVImax - NDVImin))^2 \tag{5}$$

NDVI max. is the NDVI for vegetation, and NDVI min. is the NDVI for soil.

5- Water entities have a very constant emissivity when compared to terrestrial surfaces. The NDVI, which is wavelength-based, can be used to determine the emissivity of different land surfaces in the 10 to 12 m range. The initial equation proposed was as follows [21]:

$$E = 0.004 \times PV + 0.986 \tag{6}$$

where E is the land surface emissivity from NDVI.

6- LST was computed using Equation (7) based on the BT value of the thermal band. E is derived from PV and NDVI [20]:

$$LST = \frac{BT}{1 + \left(\frac{\lambda BT}{P}\right) \ln E} - 273.15 \tag{7}$$

where: LST is land surface temperature in Celsius, λ is the average wavelength, and E is the emissivity.

P = Constant value obtained by the formula P = hc/σ is 1.438×10^{-34} Js.

where; h is Planck's constant (6.626×10^{-34} Js), c is the speed of light (2.9979246×10^{8} m/s), and σ is Stefan-Boltzmann constant (5.6697×10^{-8} W m^{-2} K^{-4}).
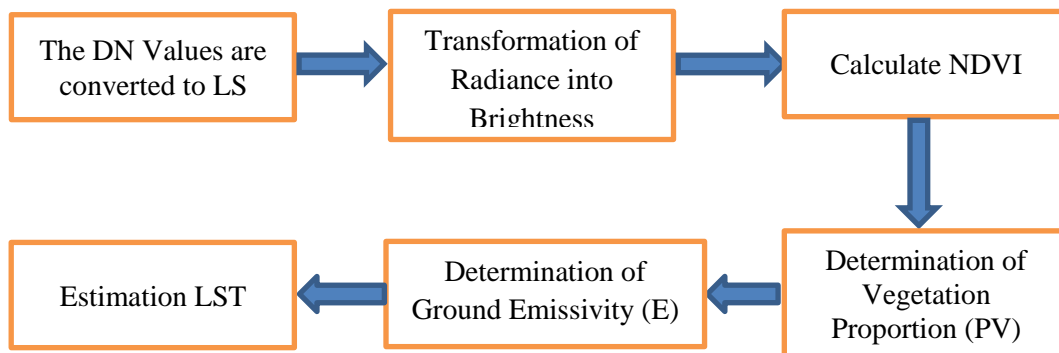

Figure 1: Methodology of this study using Landsat data.

4. Study Area

The southernmost region of Iraq is Basra, which is located between the latitudes of 31°16'49"N and 29°7'28"N and the longitudes of 46°34'30E and 48°36'34"E. It shares boundaries with Saudi Arabia, Kuwait, and Iran. The Shatt Al-Bedouin stream joins the vast desert expanse to the south, which is framed by the intersection of the Tigris and Euphrates waterways at Al-Qurnah and empties into the Arabian Bay. There are numerous lakes around Al-Qurnah and Al-Medina, and marshland extending from the north of the governorate into the governorates of Thi-Qar and Missan, which are adjacent. Iraq's legitimate entry into the ocean is through the governorate. The governorate of Basrah, like its surrounding district, has a hot and dry climate, as shown in Fig. 2.
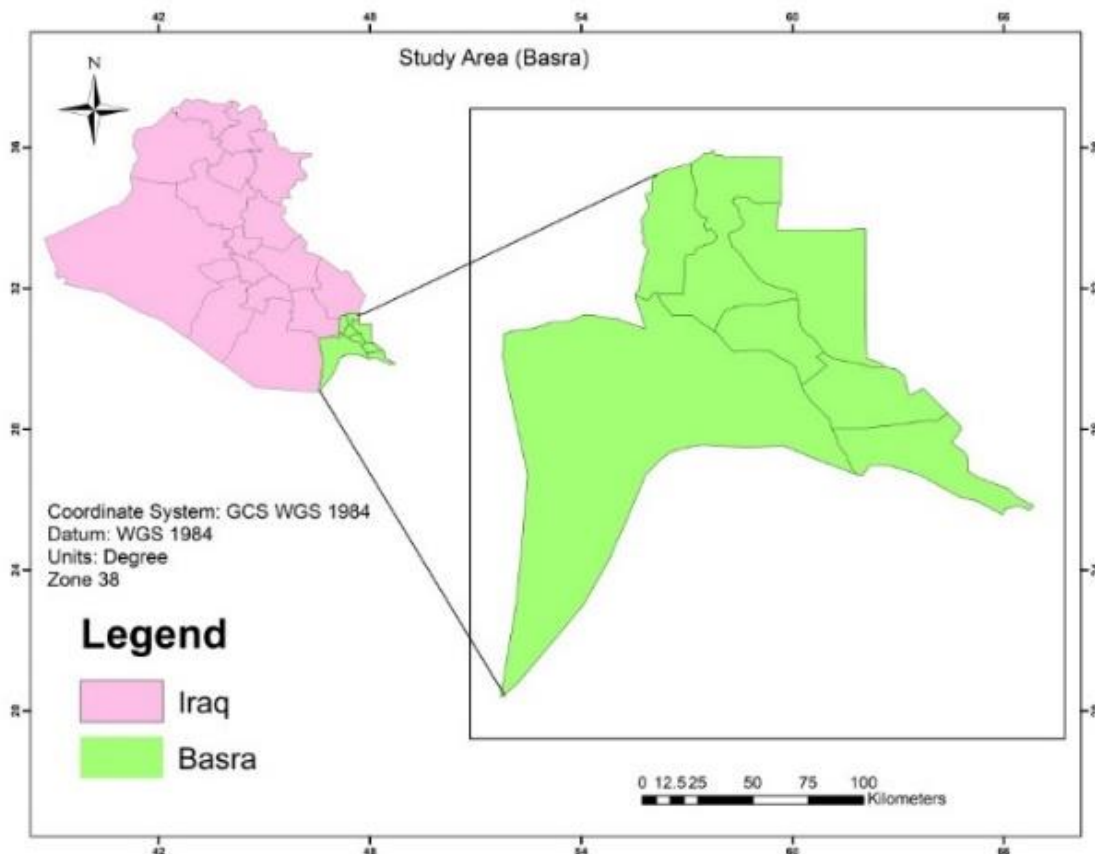

Figure 2: The Study Area in the Basra province.

5. Satellite Imagery Acquisition

In this study, ArcGIS v10.8 was employed, and the satellite data was loaded from the USGS Earth Explorer database. Landsat 8 OLI/TIRS, from Collection 2/ Level 1 as shown in Table 1.

Classification is the most critical stage in digital image processing information is extracted from the image in the Supervised Classification (Maximum Likelihood Classification (MLC) process used in bands (2, 3, 4) with a ground resolution of 30 meters from the sensor as shown in Table 2.

Table 1: Information about the data acquisition that was utilized.

Satellite Image	Sensor	Image level	Path/Row	Acquisition Data	cloud cover	Source
Landsat-8	Operational Land Image (OLI)/TIRS	Collection 2/ Level 1	166/ 38	28-07-2013	0.01	USGS Earth Explorer Database
			166/ 39	28-07-2013	0.04	
			166/ 40	28-07-2013	0.00	
			165/ 39	21-07-2013	0.00	
			166/ 38	03-12-2013	0.63	
			166/ 39	03-12-2013	1.14	
			166/ 40	03-12-2013	0.07	
			165/ 39	28-12-2013	0.54	
			166/ 38	18-07-2021	0.00	
			166/ 39	18-07-2021	0.00	
			166/ 40	18-07-2021	0.00	
			165/ 39	11-07-2021	0.00	
			166/ 38	09-12-2021	0.23	
			166/ 39	09-12-2021	0.08	
			166/ 40	25-12-2021	0.43	
			165/ 39	25-12-2021	0.5	

Table 2: Bands that are utilized to create classification maps.

Landsat 8 (OLI and sensor TIRS)	Wavelength (μm)	Resolution (m)
Band 2	0.45-0.51	30
Band 3	0.53-0.59	30
Band 4	0.64-0.67	30

6. Experimental Work

Satellite images were loaded from the USGS site. Utilizing four classes in ArcGIS 10.8, the studied area was classified using the maximum likelihood technique (vegetation, water, urban, soil). Results are shown in Fig. 3.

Using this technique of classification, the area of each class was measured and is shown in Tables 3, 4, 5 and 6.

In the next step, the LST is calculated, where the information was used to calculate the radiation of the two thermal bands 10 and 11 and to calculate the seasons of Landsat 8 satellite images for the months of July and December of 2013 and 2021 with a ground resolution of 30 meters from the sensor, as shown in Fig. 4.
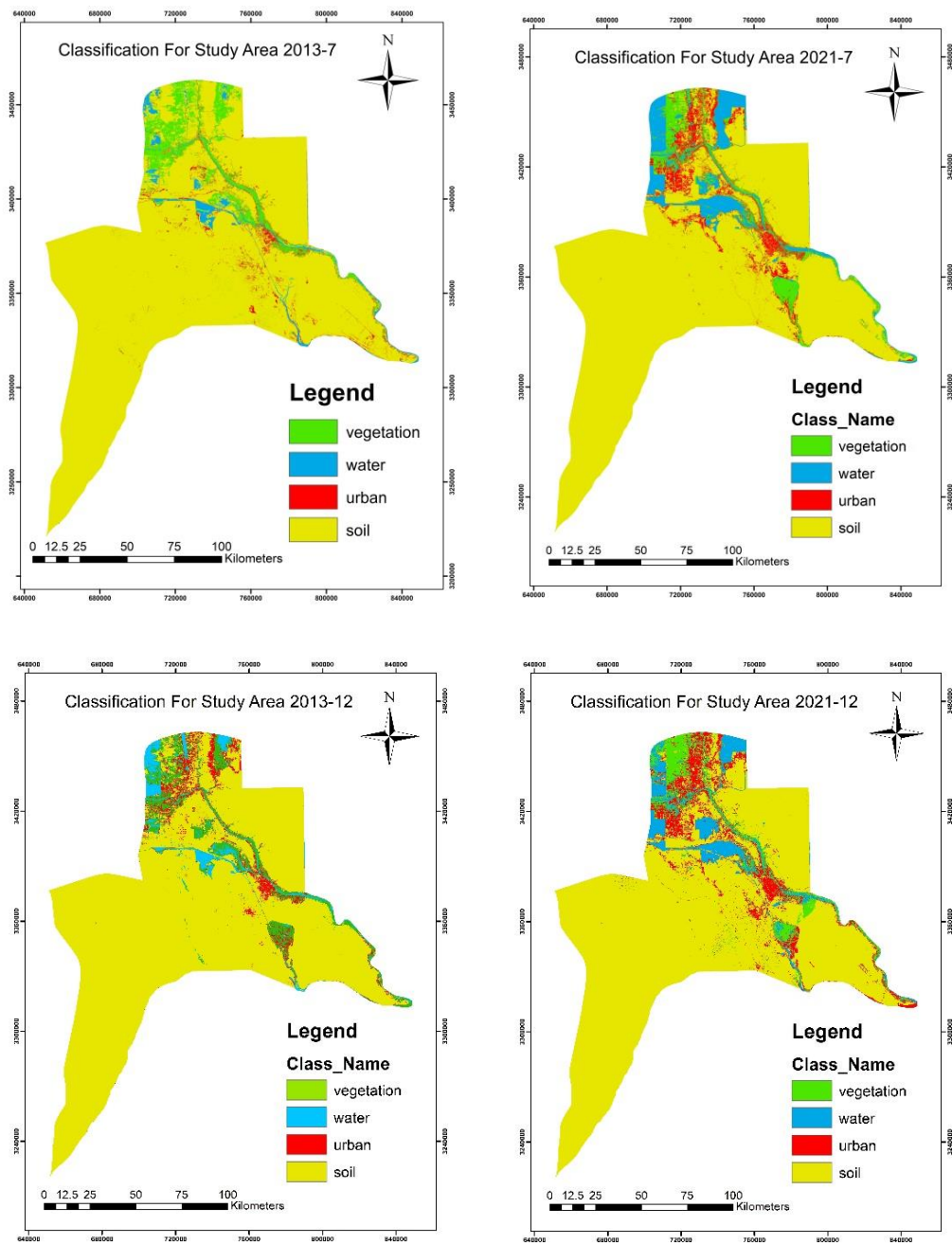
Figure 3: Classification of the studied area.

Table 3: Land covers area of 2013-7.

Categories	Year	Area in km^2
vegetation		1156.4
Water	2013-72	404.5
Urban		631.4
Soil		14944

Table 4: Land covers area of 2021-7.

Categories	Year	Area in km^2
vegetation		916.31
water	2021-7	1319.177
Urban		715.01
Soil		14484.15

Table 5: Land covers area of 2013-12.

Categories	Year	Area in km^2
Vegetation		787.203
Water	2013-12	603.06
Urban		1057.37
Soil		14984.74

Table 6: Land covers area of 2021-12.

Categories	Year	Area in km^2
vegetation		982.74
water	2021-12	1056.81
Urban		11270.02
Soil		14267.68

7. Results

7.1. Land use/cover change

To identify changes in the land cover in the province of Basra between the years (2013 and 2021), the data were extracted based on remote sensing and geographic information systems. The accuracy of the LULC images was 95% for July and 83.33% for December in 2013, and 93.2%, 86.67% in 2021 for the same months. Additionally, the LULC image Kappa statistic for July and December 2013 was 0.93 and 0.77, respectively, and for the same months in 2021, it was 0.91 and 0.81. A total of 100 reference points that represent all land use and cover were used to assure assessment accuracy. Google Earth images were used as reference data to check the accuracy of the classified images. The supervised classification results showed a variation in the land cover in terms of area due to the climate changes of the studied area and the impact of human activities. During the study period, the area of vegetation for July 2013 was observed to be 1156.4 km^2; in July 2021, it was 916.31 km^2; in December 2013, 787.203 km^2 and in December 2021, 982.74 km^2, as shown in Fig. 3 and Tables 3, 4, 5 and 6. This change in vegetation cover depends on several reasons, including rain, human activity and overgrazing.

Analyzing satellite images and calculating water areas inside the province of Basra during the study years, it was found that the water area for July 2013 reached 404.5 km^2, it increased in July 2021, reaching 1319.177 km^2, 603.06 km^2 in December 2013 and increased in December 2021 reaching 1056.81km^2. These changes in water bodies for 2013 and 2021 are shown in Fig. 3 and Tables 3, 4, 5 and 6. They are the result of two main factors: the precipitation rate and evaporation.

A continuous increase in the urban category was verified during the study period. Most of this increase was observed in 2021. In July and December 2013, it reached 631.4 km^2, and 1057.37 km^2, respectively; in July and December 2021, it reached 715.01 km^2 and 11270.02 km^2, respectively, as shown in Fig. 3 and Tables 3, 4, 5 and 6. These results correspond significantly to the reality of the annual rate of population increase in the Basra Province, where variation was observed from time to time due to human economic conditions successively affecting Iraq during the study period, significantly affecting urban expansion in the studied area.

The soil area in July 2013 reached 14944 km^2, decreased in July 2021 to 14484.15 km^2, reached 14984.74 km^2 in December 2013 and decreased in December 2021 to 14267.68 km^2. The soil in 2013 was more area than it was in 2021. The reason is the vast area of barren soil caused by land degradation, probably due to economic, safety and other problems that led to leaving the ground unattended, as shown in Fig. 3 and Tables 3, 4, 5 and 6.

7.2. Land Surface Temperature LST Change

The analysis of the Landsat thermal images showed seasonal changes in LST throughout the province of Basra. In July 2013, it ranged between (26.061°C and 95783°C); in July 2021, it was (28.812°C and 87.682°C; in December 2013, (89.72°C and 11.26°C); and in December 2021 (7.501°C and 94.881°C), as shown in Fig. 4. There was a significant increase in LST during the study period. The temperature was low in December and increased in July for 2013 and 2021. The lowest LST was found in water bodies such as rivers and lakes, while the highest LST was concentrated in buildings. The LST has a direct relationship with buildings, this means the increase the buildings the higher the LST. However, the very high temperature, which ranged between (65°C and 95.78°C), has no relation to LULC. This high-temperature results from the presence of gas flaring areas in the studied area. Gas flaring areas were identified, as shown in Fig. 5.

7.3. The Correlation between LST and LULC

The correlation coefficient R^2 between temperature and vegetation cover NDVI was 0.21123 for July and 0.10403 for December 2013. The correlation coefficient for July was 0.21602 and 0.15047 for December 2021, as shown in Fig. 6. These correlation coefficient values suggest a weak positive correlation between vegetation index and LST in Basra Province. This means that as the vegetation index increases, the LST also tends to increase, but the strength of this relationship is very weak. There could be several factors contributing to this weak correlation. One possible explanation is that the urban environment of Basra Province, such as the presence of buildings and paved surfaces, may have a dominant influence on the land surfaces temperature, for they absorb and retain heat. This could weaken the relationship between vegetation and LST as vegetation may not have as much of an impact on temperature as other factors. Another possibility is that the vegetation in Basra city is not very dense or diverse, which could limit its ability to regulate temperature. In this case, even if the vegetation index increases slightly, it may not have a large effect on LST. Overall, the weak positive correlation between the vegetation index and LST in Basra city suggests that

other factors beyond vegetation strongly influence land surface temperature in this area. The correlation coefficient R^2 between temperature and urban NBDI for July was 0.75305 and 0.60855 for December 2013; and for July, it was 0.83344 and 0.63056 for December 2021, as shown in Fig. 7. The correlation coefficient values between the urban index and the LST in Basra indicate a strong positive correlation between the two variables. This means that as the construction index increases, there is a tendency for the LST to increase as well. The high strength of the correlation coefficient indicates that the relationship between the construction index and the LST ratio in Basra is significant and likely to be caused by a direct relationship between the two variables.
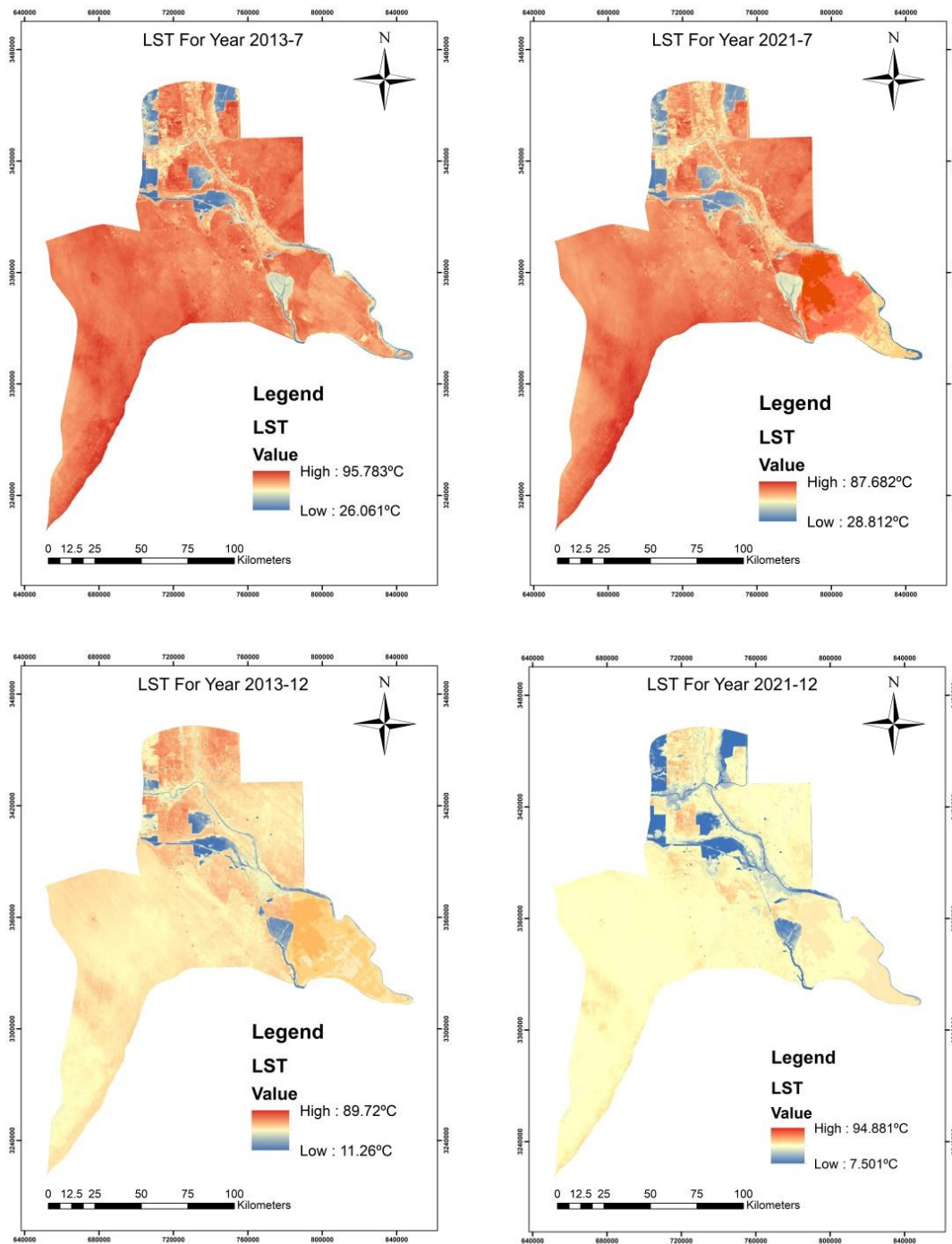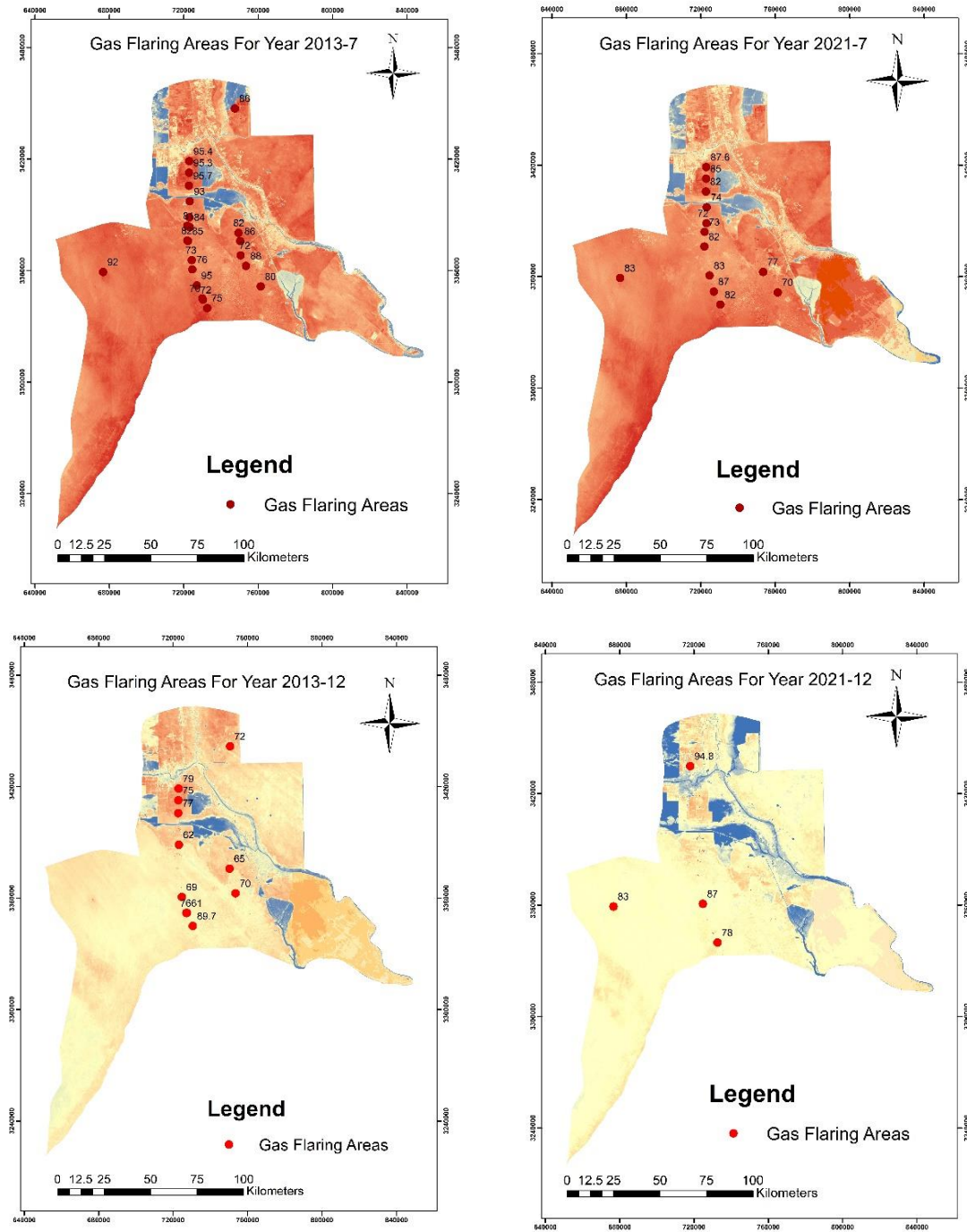

Figure 4: LST for 2013 and 2021.
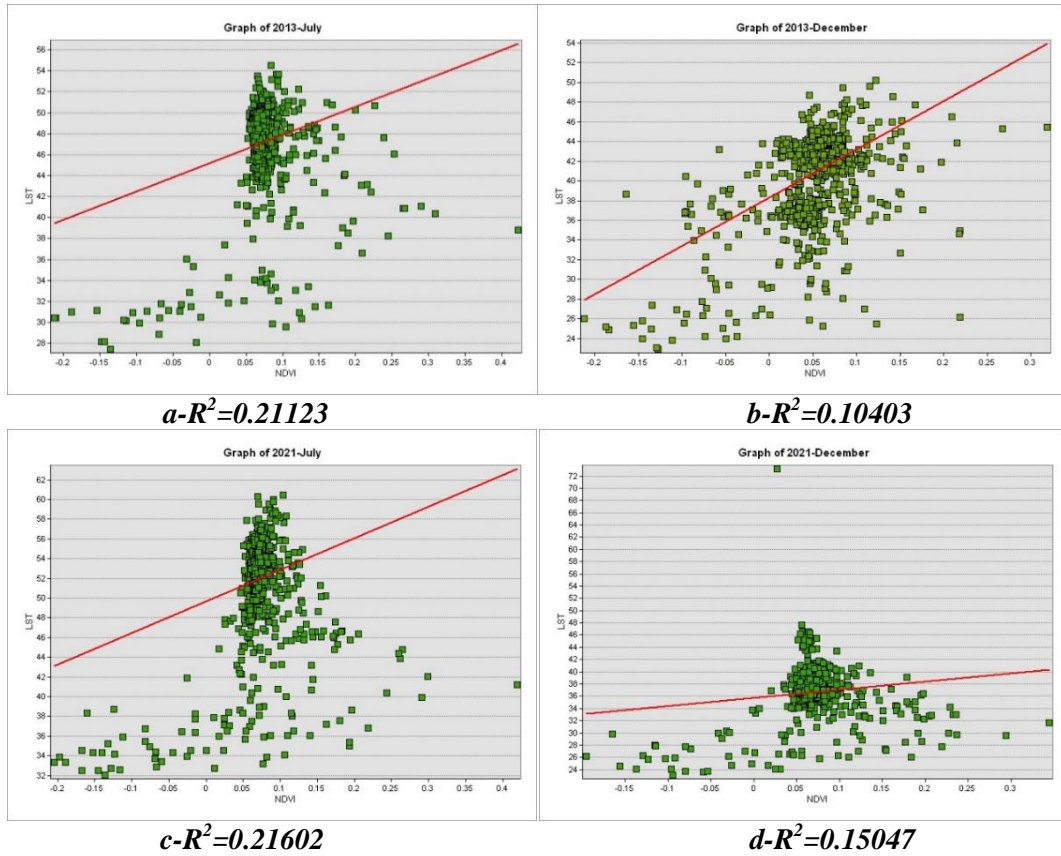
Figure 5: The Gas Flaring Areas for 2013 and 2021.

a-R²=0.21123   *b-R²=0.10403*

c-R²=0.21602   *d-R²=0.15047*

Figure 6: (a, b, c, d) The correlation LST and NDVI for 2013 and 2021.

a-R²=0.75305   **b-R²=0.60855**
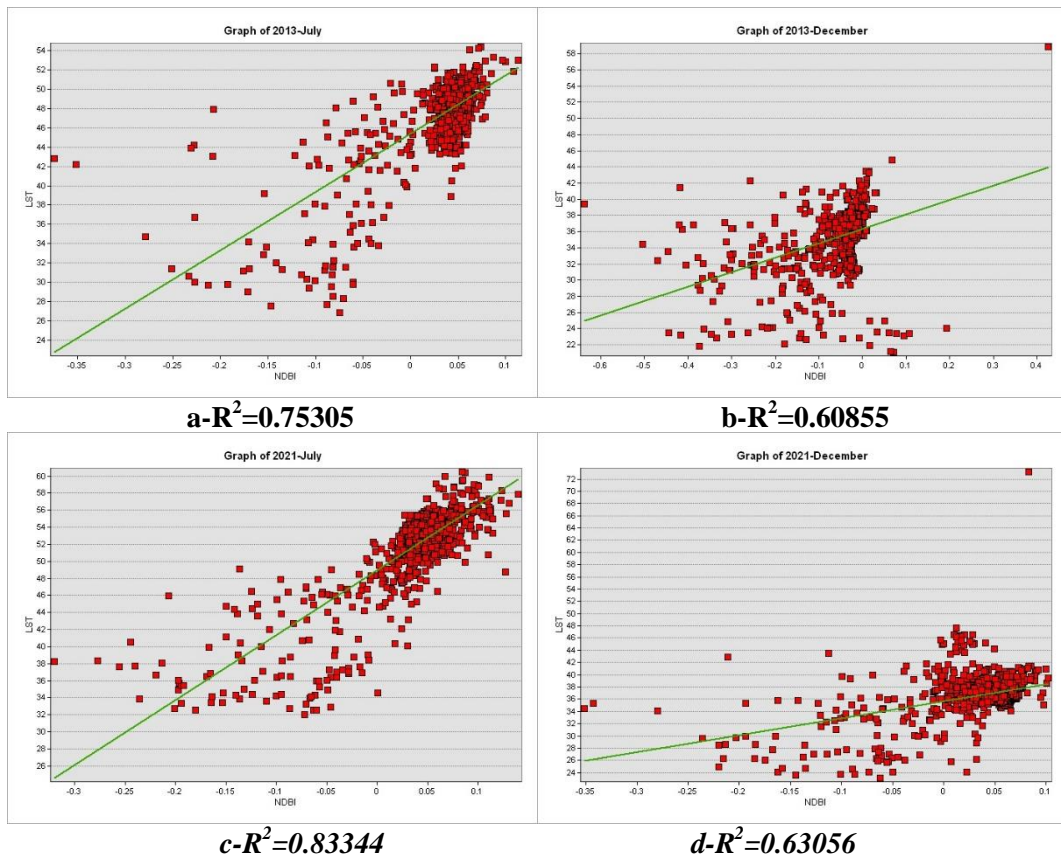
c-R²=0.83344   **d-R²=0.63056**

Figure 7: (a, b, c, d) The correlation LST and NDBI for 2013 and 2021.

8. Conclusions

Remote sensing technology was used in this study to monitor the effects of the change in LULC on LST in Basra. LST and LULC were extracted from Landsat 8 OLI/TIRS data (2013 and 2021), and statistical analysis was performed to determine any logical connection between them. When classifying LULC, the maximum likelihood classification has proven to be a very effective technique. Four LULC classes (vegetation, water, urban, and soil) were identified. There is a weak positive correlation between LST and NDVI. LST had a close relationship with both the abstract and the constructed foundations of the LULC case. Elevated LST sites included built-up areas such as central business districts, industrial areas, informal settlements, and vacant lots. The findings also indicate a strong relationship between LST and LULC, which shows several elements of environmental influence related to the urbanization trend in Basra. LST density has increased as a result of continuous and significant changes in LULC caused by urban sprawl. LST density has increased as a result of the continuous and significant changes in LULC brought about by urban sprawl. While areas with very high LST content were identified, they are gas-flaring areas in the studied area.

Acknowledgements

Conflict of interest

Authors declare that they have no conflict of interest.

References

1. J. Mallick, Y. Kant, and B. Bharath, J. Ind. Geophys. Union **12**, 131 (2008).
2. F. K. M. Al Ramahi, M. S. Jasim, and M. J. Rasheed, Ecology, Envir. Conser. **26**, 446 (2020).
3. Z. Sun, R. Ma, and Y. Wang, Envir. Geo. **57**, 1825 (2009).
4. F. K. M. Al-Ramahi, M. H. Hasan, and A. A. Zaeen, Iraqi J. Sci. **63**, 3236 (2022).
5. B. A. Ahmed and G. S. Hadi, J. Phys.: Conf. Ser. (IOP Publishing, 2021). p. 012017.
6. F. K. Mashee, O. H. Mutlag, and M. J. Rasheed, Eur. Asian J. Bio. Sci. **14**, 3367 (2020).
7. Y. K. Moussa and A. A. Alwehab, Iraqi J. Sci. **63**, 5072 (2022).
8. M. J. Rasheed and F. K. M. Al-Ramahi, Iraqi Geo J. **54**, 69 (2021).
9. A. F. Nori and F. G. Mohammed, J. Phys.: Conf. Ser. (IOP Publishing, 2020). p. 012150.
10. J. A. Richards, *Remote Sensing Digital Image Analysis*. 6th Ed. (Switzerland, Springer Cham, 2022).
11. H. K. Hammood, F. K. M. Al Ramahi, and H. S. Hussain, Iraqi J. Sci. **63**, 897 (2022).
12. R. Neware, Envir. Earth Sci.: Remot. Sens., 2019030122 (2019).
13. K. Perumal and R. Bhaskaran, J. Comp. **2**, 124 (2010).
14. A. A. Salman and F. K. M. Al Ramahi, Iraqi J. Sci. **63**, 5589 (2022).
15. J. P. Walawender, M. J. Hajto, and P. Iwaniuk, Inter. Geosci. Rem. Sens. Symposium (IEEE, 2012). p. 4371.
16. A. N. Abdul-Hammed, Iraqi J. Sci. **63**, 1394 (2022).
17. J. W. Rouse, R. H. Haas, J. A. Schell, and D. W. Deering, NASA Spec. Publ. **351**, 309 (1974).
18. K. Ali, K. Fouad, B. Abdul-Rahman, and Cons, Eco. Env. Cons. **25**, S44 (2019).

19. T. A. Dhamin, E. Khanjer, and F. Mashee, MINAR Int. J. Appl. Sci. Technol., 57 (2020).
20. Z. Wan, Y. Zhang, Q. Zhang, and Z.-L. Li, Inter. J. Rem Sens. **25**, 261 (2004).
21. Z. Wan, Atmosph. Clim. Sci. **4**, 1 (1999).

مراقبة درجة حرارة سطح الأرض (LST) والغطاء الأرضي لمحافظة البصرة باستخدام تقنية الاستشعار عن بعد ونظام المعلومات الجغرافية

كوثر سلمان[1] و بان عبد الرزاق [1]

[1]قسم التحسس النائي، كلية العلوم، جامعة بغداد، بغداد، العراق

الخلاصة

تحققت هذه الدراسة في التغيير الذي يحدث في محافظة البصرة بأستخدام الأساليب الجغرافية المكانية وتحليل الاختلافات في درجة حرارة سطح الارض بين أنواع مختلفة من الغطاء الأرضي. في شهري تموز وكانون الأول في عامي 2013 و 2021، تم استخدام صور لاندسات في Landsat 8 OLI / TIRS، وتمت معالجة صور الأقمار الصناعية باستخدام برنامج ArcGIS 10.8. تم إنشاء فئات الدراسة لاستخدامات الأراضي والغطاء الأرضي من خلال تطبيق تقنيات التصنيف الخاضعة للإشراف، وتم حساب درجة حرارة سطح الأرض باستخدام بيانات من درجة حرارة سطوع جهاز استشعار الأقمار الصناعية. وفقًا لنتائج الدراسة، كانت هناك زيادة في المناطق الحضرية (بما في ذلك الأراضي القاحلة). من 2013 إلى 2021، تم العثور على ارتباط أكبر بين الأراضي الحضرية و LST، مما يشير إلى زيادة تأثير جزيرة الحرارة الحضرية السطحية. كما يتضح من معاملات الارتباط ذات الدلالة الإحصائية، ولها تأثير كبير على التغيرات في درجة حرارة سطح الأرض. سلطت هذه الدراسة أيضًا الضوء على الاختلافات الرئيسية في كيفية تأثير استخدام الأراضي والغطاء على LST في جميع الفترات الزمنية للتحقيق. لذلك، فإن تقنيات الاستشعار عن بعد وأنظمة المعلومات الجغرافية مفيدة لتتبع وتحليل أنماط التوسع الحضري وتقييم آثارها على درجة حرارة سطح الأرض.

الكلمات المفتاحيه: استخدام الأرض الغطاء الأرضي (LULC)، درجة حرارة سطح الأرض (LST)، مؤشر الغطاء النباتي (NDVI)، تقنيات نظم المعلومات الجغرافية ، جزيرة الحرارة الحضرية.